

# Nanoscale Departures: Excess Lipid Leaving the Surface during Supported Lipid Bilayer Formation

Ling Zhu,<sup>†,‡,¶</sup> Danijela Gregurec,<sup>†,‡</sup> and Ilya Reviakine<sup>\*,†,§,||</sup>

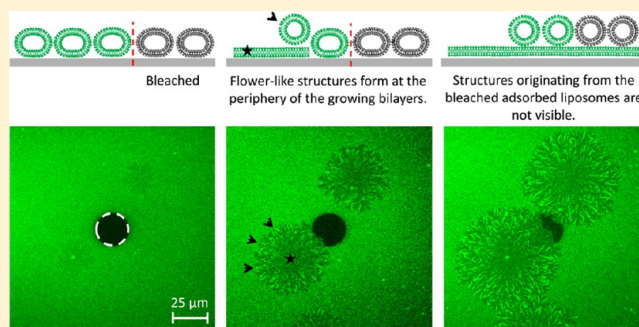
<sup>†</sup>Biosurfaces, CIC biomaGUNE, Paseo Miramón 182, 20009 San Sebastián, Spain

<sup>‡</sup>Department of Biochemistry and Molecular Biology, University of the Basque Country (UPV/EHU), 28940 Leioa, Spain

<sup>§</sup>Faculty of Engineering, University of the Basque Country (UPV/EHU), Alameda Urquijo s/n, 48013 Bilbao, Spain

## Supporting Information

**ABSTRACT:** The behavior of small liposomes on surfaces of inorganic oxides remains enigmatic. Under appropriate conditions it results in the formation of supported lipid bilayers (SLBs). During this process, some lipids leave the surface (desorb). We were able to visualize this by a combination of time-resolved fluorescence microscopy and fluorescence recovery after photobleaching studies. Our observations also allowed us to analyze the kinetics of bilayer patch growth during the late stages of SLB formation. We found that it entails a balance between desorption of excess lipids and further adsorption of liposomes from solution. These studies were performed with liposomes containing zwitterionic phospholipids (dioleoylphosphatidylcholine alone



or a mixture of dioleoylphosphatidylcholine, dipalmitoylphosphatidylcholine, and cholesterol) on TiO<sub>2</sub> in the presence of Ca<sup>2+</sup> but in the absence of other salts.

## INTRODUCTION

The preparation of surface-supported lipid bilayers, or SLBs,<sup>1</sup> from liposomes, is experimentally a very simple procedure (Figure 1, and Figure S1 in the Supporting Information). On the other hand, the mechanism behind the process turned out to be far more challenging to understand.<sup>2</sup> SLBs themselves are routinely used in biophysical studies and as platforms in biosensor and biotechnology research.<sup>1,3,4</sup> However, lack of control over essential parameters that govern their formation continues to limit their usefulness.

SLBs form spontaneously from adsorbing liposomes of appropriate compositions on surfaces of some hydrophilic, smooth materials such as glass or silica, mica, silicon nitride, and titania. During the formation process, some of the lipids may leave the surface (Figure 1). There are several arguments and lines of evidence for this. A layer of surface-adsorbed liposomes that serves as a precursor to the SLB may contain more lipids than needed to form a confluent SLB. The amount of lipid excess depends on the number of parameters, including liposome surface coverage and the rate at which they rupture to form bilayers. For a layer of 25 nm liposomes adsorbed on the surface at the random close packing limit of  $\sim 0.55$ ,<sup>5</sup> there are  $\sim 1.6\times$  more lipids than needed to cover the surface of the same area with a confluent bilayer (in this calculation, the area per lipid was taken as  $0.72 \text{ nm}^2$ <sup>6</sup> and the number of lipids per liposome was calculated from the areas of the outer and inner leaflets assuming a bilayer thickness of  $\sim 3.7 \text{ nm}$ <sup>7</sup>).

While the surface coverage required for SLB formation need not be as high as used in this simplistic example, several

experimental findings do support the notion that there is lipid excess at the surface during SLB formation. During their measurements of SLB formation with a combined quartz crystal microbalance-surface plasmon resonance (QCM-SPR) instrument, Reimhult et al. showed loss of lipid mass from the surface.<sup>8</sup> Lipid loss was greater at higher liposome concentrations, because of the increased transport rate, and when larger liposomes were used, because larger liposomes bring more lipids to the surface for the same surface coverage. This arises from the curvature effects discussed in detail by Huang et al.<sup>7</sup> and by Richter et al. in the supporting information of ref 9. Weirich et al. similarly observed lipid loss during the SLB formation process followed by fluorescence microscopy.<sup>10</sup> These authors also conclude that the details of this process are sensitive to the lipid concentration in solution, but they additionally observed spatial heterogeneity, suggesting sensitivity to the local liposome organization or concentration at the surface. Further evidence came from ellipsometric measurements.<sup>11</sup> These authors once again observed that higher solution concentrations lead to more pronounced desorption and suggested that it was the rate-limiting step in the SLB formation at least under some conditions.<sup>11</sup> All of these studies were performed on SiO<sub>2</sub> with various phosphatidylcholine liposomes—the most commonly studied system. What remains unclear is the form in which the lipids depart and the effect this

Received: April 10, 2013

Revised: October 25, 2013

Published: November 22, 2013

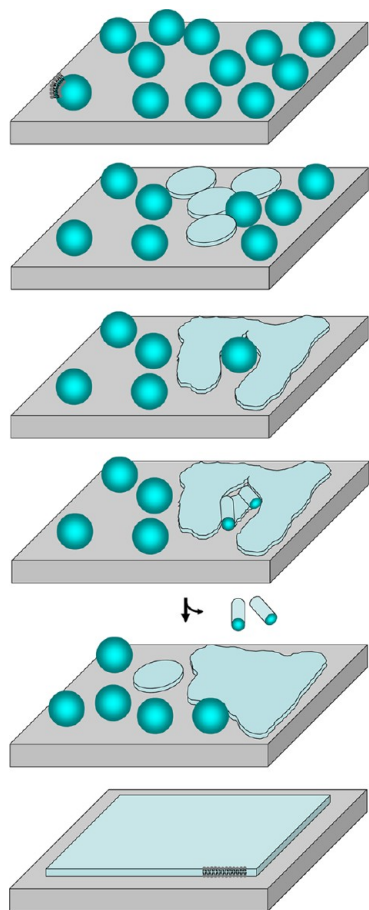


**Figure 1.** Formation of supported lipid bilayers (SLBs) from adsorbed liposomes involves lipid loss from the surface. Adsorbed liposomes (top) rupture to form lipid bilayer patches (light blue discs) that coalesce and grow, eventually covering the entire surface with a homogeneous bilayer (bottom). However, a layer of adsorbed liposomes contains more lipids than can be accommodated on the surface in the form of a bilayer. The manner in which excess lipids may leave is illustrated in the second drawing from the bottom, where a rupturing liposome surrounded by the lipid patch locally leads to an excess of lipids. The figure is not to scale. A 2D version of this illustration is shown in Figure S1 in the Supporting Information.

process has on the overall kinetics of the SLB formation. We report here essentially new observations that shed some light on these issues.

## MATERIALS AND METHODS

**Materials.** Dioleoylphosphatidylcholine (DOPC), dipalmitoylphosphatidylcholine (DPPC), cholesterol, and chain-labeled 18:1-12:0 NBD-PC were purchased from Avanti Polar Lipids (Alabaster, AL) in powder form. They were stored at  $-20\text{ }^{\circ}\text{C}$ . Lipid stock solutions were prepared by dissolving the lipid powder in chloroform in clear glass vials with solid caps with a PTFE liner (Sigma-Aldrich, Madrid, Spain) and stored at  $-20\text{ }^{\circ}\text{C}$ . Lipid concentration in the stock solutions was checked by phosphorus assay following the protocol from Avanti Polar Lipids.

The buffer used for liposome preparation and deposition throughout this study was made of 10 mM HEPES and 2 mM  $\text{CaCl}_2 \cdot 6\text{H}_2\text{O}$ . pH was adjusted with NaOH to 7.4. Nanopure water used was produced with a Diamond UV water purification system (Branstead International, IA). The chemicals, ( $\geq 99.0\%$  purity) were purchased from Sigma-Aldrich (Madrid, Spain), except for NaOH which was purchased from Scharlab (Barcelona, Spain).

**Methods. Liposome Preparation.** Two kinds of liposomes were used in this study: one consisting of DOPC and another consisting of a mixture of DOPC, DPPC, and cholesterol at a molar ratio of 35:35:30. Both were doped with 1 mol-% of NBD-PC. They were prepared by sonication.<sup>12</sup> First, appropriate amounts of lipid stock solutions were mixed in round-bottom glass test tubes. Chloroform was evaporated with a stream of argon to form thin lipid films on the tube walls. Lipid films were further dried under vacuum generated with an oil-free diaphragm pump for 1 h. The dry lipid films were rehydrated by vigorous vortexing in buffer at a final lipid concentration of 2 mg/mL. The resulting MLV suspensions were subjected to sonication with a tip sonicator (Brandson, USA) in pulsed mode at 30% duty cycle under a nitrogen atmosphere. DOPC liposomes were sonicated in an ice-water bath for 1 h. DOPC:DPPC:cholesterol liposomes were sonicated at  $60\text{ }^{\circ}\text{C}$  (above the transition temperature of DPPC which is  $41\text{ }^{\circ}\text{C}$ <sup>13</sup>) for 3 h.

Sonicated liposome solutions were cleared of titania particles by centrifugation at 60 000g for 3 h at  $4\text{ }^{\circ}\text{C}$  for DOPC and at room temperature for DOPC:DPPC:cholesterol (35:35:30).

Liposome sizes and size distributions were characterized by dynamic light scattering (DLS) with the Zetasizer (Malvern, UK) and were bimodal, as expected,<sup>12</sup> with the sizes of  $\sim 30$  and  $150$  nm for DOPC and  $\sim 50$  and  $170$  nm for DOPC:DPPC:cholesterol (35:35:30). Sonicated liposomes were kept at  $4\text{ }^{\circ}\text{C}$  for DOPC and room temperature for DOPC:DPPC:cholesterol (35:35:30) for no more than 1 week. Storing liposomes for this amount of time did not affect SLB formation experiments.

Some of the liposome solutions were examined by DLS and CryoTEM as late as 4 weeks after the preparation, and they still contained significant populations of small liposomes. However, preparations older than 1 week were not used in the bilayer formation experiments except for the one experiment described in the Supporting Information, Figure S7, in which a 3 month old liposome suspension was used to specifically test the effects of liposome aging on the observations reported here. DLS measurements of these liposomes revealed two peaks,  $32 \pm 2$  and  $93 \pm 6$  nm, but the suspension also contained larger aggregates, making the size determination somewhat less reliable.

**Substrate Preparation, Cleaning and Characterization. Substrate Preparation.** Twenty-five mm and 12 mm  $\text{TiO}_2$ -coated glass coverslips were prepared by direct current (dc) magnetron reactive sputtering in an ATC 1800 UHV sputtering system (AJA International Inc., MA) equipped with a load-lock transfer chamber. The base pressure in the chamber was kept at  $\sim 1.2 \times 10^{-8}$  Pa. Prior to the deposition process, glass slides were cleaned for 10 min at  $50\text{ }^{\circ}\text{C}$  in a mixture of  $\text{H}_2\text{O}:\text{NH}_4\text{OH}:\text{H}_2\text{O}_2$  at a 1.5:1:1 volume ratio, followed by a rinse with nanopure water, and another 10 min at  $50\text{ }^{\circ}\text{C}$  in a mixture of  $\text{H}_2\text{O}:\text{HCl}:\text{H}_2\text{O}_2$ , also at a 1.5:1:1 volume ratio. Clean slides were rinsed in nanopure water and dried under a stream of nitrogen. They were then installed in the sputtering plant where they were further cleaned in argon plasma generated with a negative radio frequency (rf) bias of 162 V in a 4 Pa argon atmosphere for 3 min.

Film deposition was carried out by the protocol adapted from ref 14. Briefly, a 2 in. diameter Ti target (99.99% purity, AJA International Inc., MA) was used, with a power of 228 W, in the argon/oxygen atmosphere generated by combining 10 sccm of argon flow with 20 sccm of oxygen flow at 0.4 Pa working pressure. Substrate-to-target distance was kept at 4 cm and the substrates were rotated at 80 rpm. The sputtering was performed at room temperature for 120 min, resulting in transparent  $\text{TiO}_2$  films of  $\sim 30$  nm thickness. Film thickness was calculated based on the sputtering rate of 0.42 nm/s measured with a built-in QCM sensor under identical conditions and verified by optical ellipsometry. Surface chemical composition of the films was analyzed by X-ray photoelectron spectroscopy (XPS) after cleaning. Surface roughness was characterized by atomic force microscopy, performed with Nanoscope V Multimode atomic force microscope (Santa Barbara, CA) in air (Figure S2 in the Supporting Information).

**Surface Cleaning.** Surfaces were cleaned in 2% SDS solution for 30 min, rinsed with Nanopure water, blow-dried with nitrogen, and

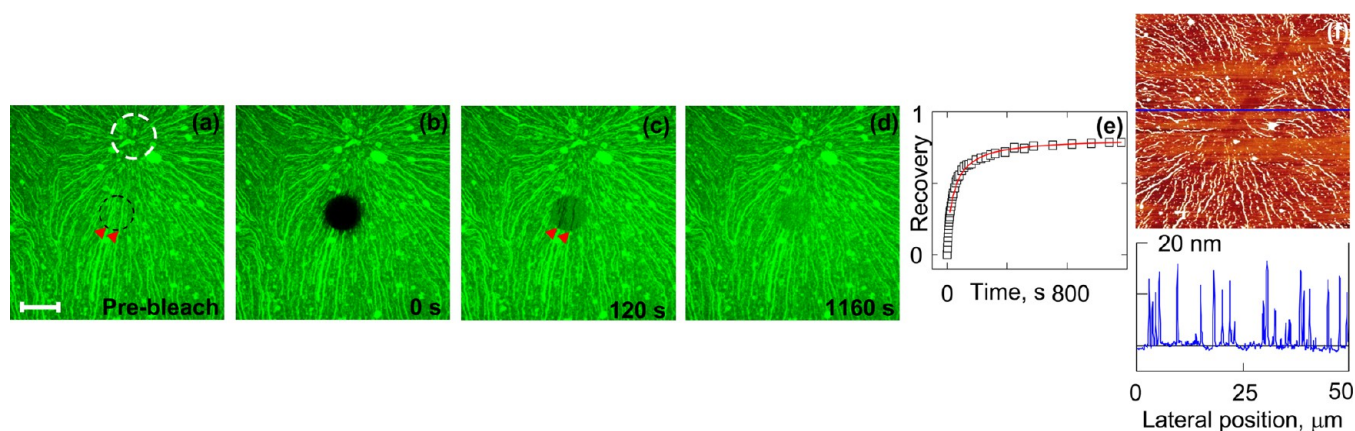


**Figure 2.** Example of an SLB coexisting with extended structures. These images were obtained with samples prepared from liposomes containing DOPC, DPPC, and cholesterol at the molar ratio of 35:35:30 labeled with 1% NBD-PC on titania in a buffer containing 10 mM HEPES and 2 mM  $\text{CaCl}_2$ , pH 7.4, at room temperature. (a–d) Fluorescence microscopy images illustrating lipid organization and the photobleaching series. White dashed circle in (a) indicates the area where the tubular structures appear to originate or terminate. Black dashed circle corresponds to the area that will be photobleached; it appears dark in (b), (c), and (d). The fluorescence intensity recovers, as expected for an SLB, but the recovery is incomplete. Tubular structures are not visible in the bleached area in (c), but there are dark lines in places where they were located. These dark lines are indicated with red arrowheads in (c), while the original structures are indicated with red arrowheads in (a). The dark lines are mostly gone in (d). Scale bar in (a) is  $25 \mu\text{m}$ . (e) Recovery of the fluorescence intensity in the bleached area fitted with the Soumpasis equation. (f) Atomic force microscopy depicting the tubular structures. The area in their center is relatively devoid of them. Blue line indicates where the height profile shown below the image was taken. The image is  $50 \times 50 \mu\text{m}^2$ ; Z scale 20 nm.

treated in a preheated UV-Ozone cleaning chamber (Bioforce, Nanosciences, Ames, AL) for 30 min immediately before use. The UV-Ozone treatment cleans the surface of the organic contaminants and makes the surface hydrophilic.

**Surface Chemical Composition Analysis by X-ray Photoelectron Spectroscopy (XPS).** Surface chemical composition of the  $\text{TiO}_2$ -coated substrates was analyzed by XPS in a SPECS SAGE HR 100 (SPECS, Berlin, Germany) spectrometer equipped with a Mg  $K\alpha$  (1253.6 eV) nonmonochromatic source which was operated at 12.5 kV and 250 W. The takeoff angle was fixed at  $90^\circ$  and the analysis was conducted at a pressure of  $\sim 10^{-8}$  Torr. Surfaces were brought into the XPS chamber within 5 min after cleaning/preparation. Survey spectra were obtained with a pass energy of 30 eV and detailed spectra were acquired for Ti  $2p_{3/2}$ , Ti  $2p_{1/2}$ , O 1s, and C 1s regions with a pass energy of 15 eV. Spectra were analyzed in with the CasaXPS 2.3.15dev87 software. The analysis consisted of satellite removal, Shirley background subtraction, calibration to the C 1s peak at 285 eV, and peak fitting with Gaussian–Lorentzian line shapes to determine the atomic percentages of various elements present on the surface. Freshly cleaned surfaces typically contained  $\sim 13$  atomic % of carbon and  $\sim 95$ % of the Ti  $2p$  peak could be assigned to  $\text{Ti}^{\text{IV}}$ , with  $\sim 5$ % corresponding to the lower oxidation states.<sup>15–17</sup> Samples containing extraneous elements or higher amounts of carbon (contamination) were discarded.

**Bilayer Formation Experiments.** A clean, 25 mm,  $\text{TiO}_2$ -coated glass slide was mounted in a homemade, open fluid cell consisting of a Teflon ring pressed to the glass slide with a metal clamp. A Viton O-ring was placed between the glass and the Teflon to prevent leakage. Viton O-rings were cleaned in Cobas cleaner (Roche Mannheim, Germany) for 30 min, while the Teflon rings were cleaned for 30 min in 2% Cuvette cleaner (Sigma-Aldrich, Madrid, Spain). Both were washed with copious amounts of nanopure water immediately before assembly. The assembly was performed in a laminar flow hood to reduce contamination and the fluid cell was filled with 1 mL of buffer, to which a small amount of concentrated liposome solution was added to a final lipid concentration of 0.36 mg/mL. The solutions were thoroughly mixed by repeatedly adding and removing a small volume of liquid to/from the fluid cell. Samples were incubated at  $60^\circ\text{C}$  for 1 h. After incubation, samples were rinsed with buffer and observed with fluorescence microscopy also at  $60^\circ\text{C}$ . Samples were then cooled down to room temperature for observation with fluorescence microscopy and/or atomic force microscopy at room temperature as described below.

For the experiment shown in Figure S6 in the Supporting Information, images were taken at room temperature before the samples were brought to  $60^\circ\text{C}$ .

For the time-resolved experiments (Figure 4, and Movie S3 and Figure S4 in the Supporting Information), the buffer-filled fluid cells were mounted on the stage of the fluorescence microscope at  $60^\circ\text{C}$  and then the liposomes were added. Otherwise, the procedure remained the same.

**Fluorescence Microscopy and Fluorescence Recovery after Photobleaching (FRAP).** Fluorescence and FRAP experiments were performed with a Zeiss LSM 510 laser scanning confocal microscope (Carl Zeiss, Oberkochen, Germany) equipped with a 25 mV argon laser (488 nm line was used for the excitation of the NBD fluorophore) and a  $63\times$  oil immersion objective. FRAP measurements and analysis to extract mobile fractions and diffusion coefficients were performed after Axelrod et al.<sup>18</sup> and Soumpasis et al.<sup>19</sup> The diameter of the bleached spot (round shaped) was  $22 \mu\text{m}$ . A nonbleached spot of similar size was used as a reference to account for the focus drift. The bleaching time was kept at less than 5% of the characteristic recovery time.

**Atomic Force Microscopy (AFM).** Some of the samples observed in the fluorescence microscope were also observed with a JPK Explorer atomic force microscope (JPK Instruments AG, Germany). AFM experiments were also performed with a Nanoscope V Multimode atomic force microscope (Santa Barbara, CA) equipped with a vertical engage  $120 \times 120 \mu\text{m}^2$  (“J”) scanner and a tapping mode fluid cell. For these experiments, 12 mm  $\text{TiO}_2$ -coated glass slides were used instead of the 25 mm ones. They were cleaned as described above for the fluorescence experiments and mounted on the microscope on BYTAC-covered metal disks with double-sided tape as previously described.<sup>20,21</sup> Lipid solutions were incubated on them for  $\sim 1$  h at  $60^\circ\text{C}$  in sealed water-filled Petri dishes to prevent evaporation. After incubation, the samples were rinsed, cooled down to room temperature, and installed in the AFM.

In either case, images were acquired in tapping mode, with oxide-sharpened silicon nitride tips mounted on triangular cantilevers with nominal force constants of  $\sim 0.06$  N/m (Veeco, Mannheim, Germany). Images were flattened and plane-fitted as required.

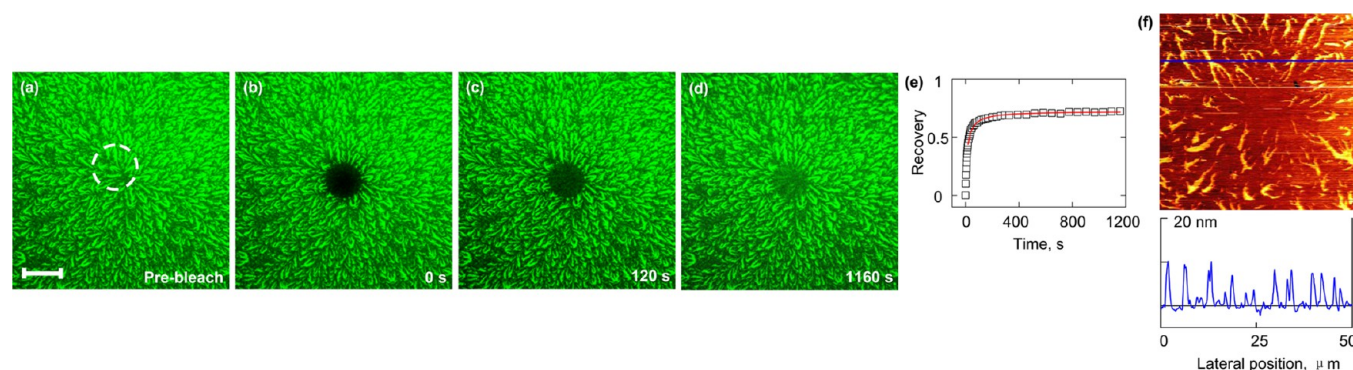


**Figure 3.** Example of an SLB coexisting with flowerlike structures. Flowerlike structures were found when DOPC liposomes were allowed to interact with  $\text{TiO}_2$  in 10 mM HEPES:2 mM  $\text{CaCl}_2$ , pH 7.4 buffer. These structures also coexist with an SLB, as is evident from the recovery behavior shown in (e). A  $50 \times 50 \mu\text{m}^2 \times 20 \text{ nm}$  AFM image of this sample is shown in (f), with the height profile shown underneath. Fluorescence images are  $142 \times 142 \mu\text{m}^2$ . White dashed circle in (a) indicates the point of origin of the flowerlike structures. All the images were taken at room temperature. Scale bar in (a) is  $25 \mu\text{m}$ .

**Table 1. Lipid Mobility<sup>a</sup>**

composition	temp ( $^{\circ}\text{C}$ )	$M$	$D \times 10^{-8} \text{ cm}^2/\text{s}$	figure
DOPC, before wash	21	$0.80 \pm 0.08$	$1.06 \pm 0.45$	Figure 3
	60	$0.77 \pm 0.06$	$1.62 \pm 0.12$	
DOPC:DPPC:cholesterol, before wash	21	$0.82 \pm 0.06$	$0.55 \pm 0.08$	Figure 2
	60	$0.73 \pm 0.03$	$1.78 \pm 0.18$	
DOPC, after wash with water	21	$1.04 \pm 0.05$	$0.54 \pm 0.03$	Figure 4
	60	$0.99 \pm 0.07$	$0.90 \pm 0.07$	
DOPC:DPPC:cholesterol, after wash with water	21	$1.01 \pm 0.07$	$0.31 \pm 0.04$	Figure 4
	60	$0.99 \pm 0.07$	$0.82 \pm 0.2$	
DOPC:DPPC	60	$1.02 \pm 0.07$	$1.86 \pm 0.32$	Figure S6
DOPC:DPPC after wash with water	60	$1.02 \pm 0.07$	$1.44 \pm 0.78$	
DOPC:DPPC in 5 mM HEPES	22	$1.03 \pm 0.04$	$0.32 \pm 0.03$	
	60	$0.99 \pm 0.05$	$1.44 \pm 0.14$	
DOPC in 5 mM HEPES	22	$1.04 \pm 0.01$	$0.58 \pm 0.03$	
	60	$1.02 \pm 0.06$	$0.91 \pm 0.07$	

<sup>a</sup>Diffusion coefficients and mobile fractions of NBD-PC label determined under various experimental conditions presented in this study. For the DOPC:DPPC:cholesterol system, the lipid composition was 35:35:30 mol %. For the DPPC:DOPC system, the lipid composition was 1:1 (by mole). Unless otherwise indicated, 10 mM HEPES:2 mM  $\text{CaCl}_2$  buffer was used to prepare bilayers.

## RESULTS

When preparing bilayers from dioleoylphosphatidylcholine (DOPC) liposomes or liposomes composed of mixtures containing DOPC, dipalmitoylphosphatidylcholine (DPPC), and cholesterol at a 35:35:30 molar ratio, on  $\text{TiO}_2$  in the pH 7.4 buffer containing 2 mM  $\text{CaCl}_2$  and 10 mM HEPES, we observed the bilayers to coexist with structures exhibiting tube- or flowerlike morphology (Figures 2, 3, and 4). These structures appeared to originate from common centers (indicated with white dashed circles in Figures 2 and 3).

SLB formation was evident from the long-range mobility of the lipids evaluated by fluorescence recovery after photobleaching. The photobleaching sequences and recovery plots for the two systems are shown in Figures 2 and 3, respectively, and the values of the mobile fractions and diffusion coefficients are collected in Table 1. The values of the diffusion coefficients are typical of SLBs,<sup>22,23</sup> taking into account that cholesterol slows down lipid diffusion.<sup>24,25</sup> However, the recovery was not complete, as is evident from relatively low mobile fractions ( $\sim 0.7$ – $0.8$ , Table 1). The tubular or flowerlike structures did not recover to the original levels of intensity. This is visible both in the DOPC:DPPC:cholesterol system (Figure 2) and in the DOPC system (Figure 3). During the recovery process,

dark (low-intensity) lines were visible in places where the original tubular structures were present (red arrowheads in Figure 2c). They are also apparent in the DOPC system (Figure 3c).

The same structures could be observed by atomic force microscopy (AFM, Figures 2f and 3f). AFM revealed that the areas where the tubular structures originated were largely devoid of them (Figures 2f and 3f). In other words, tubular structures appear at the periphery of the smooth SLB regions. The height of these tubular structures was  $\sim 10$ – $15 \text{ nm}$  above the surrounding bilayer (Figures 2f and 3f). These structures were very loosely attached to the bilayer and could be easily displaced by the tip if the force was not kept to a minimum.

Because these structures appeared at the periphery of the SLB areas, we hypothesized that they might be related to the pathway for lipid desorption from the surface during SLB formation. To investigate this idea, we acquired sequences of fluorescence images following the formation of the bilayer from DOPC liposomes (Figure 4; a Movie S3 can also be seen in the Supporting Information, and another example, from a different experiment, in Figure S4 in the Supporting Information). The process of SLB formation begins with a layer of adsorbed liposomes. This is confirmed by bleaching the fluorescence that

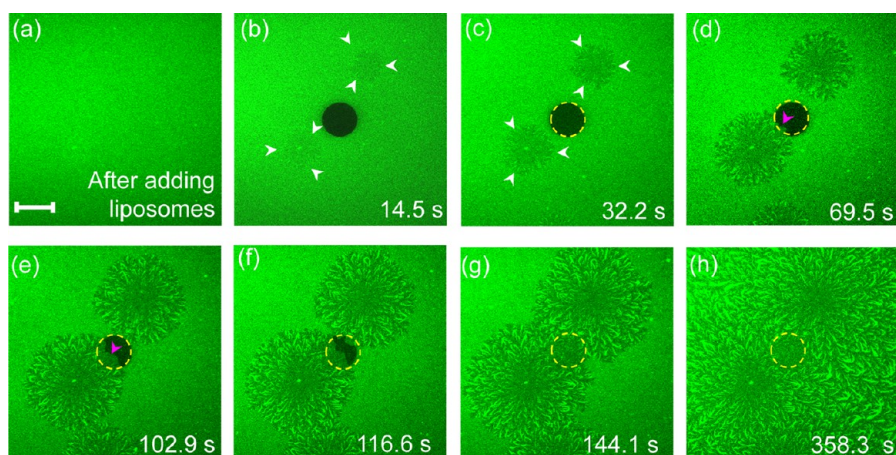


**Figure 4.** Time-resolved fluorescence images of bilayer formation. The images shown in this figure were acquired with pure DOPC liposomes in a buffer containing 10 mM HEPES and 2 mM  $\text{CaCl}_2$  at 60 °C. A supported vesicular layer is formed after adding liposomes (a). This can be judged from lack of recovery after photobleaching; the bleached spot is highlighted with a dashed gold circle in (c–h), and fluorescence intensity within that spot does not recover in images (b–d). Darker circular patches appear in (b), highlighted with the white arrowheads, that grow as a function of time until they cover essentially the entire surface (b–h). They are decorated with the flowerlike structures at the periphery, but in the centers they are free of these structures. The intensity in the bleached spot begins to recover once the darker patches extend into it (purple arrowheads in (d) and (e)). Based on that, the patches are considered to be bilayers. Note that the flowerlike structures are not visible in the bleached area (f–h). Therefore they arise from the lipids present on the surface in the adsorbed liposomes and represent the excess lipid leaving the surface during the bilayer formation. Note also that where the adjacent bilayer areas merge, the flower structures have opposite orientations. This is more clearly seen in Movie S3 and Figure S4 in the Supporting Information. Scale bar in (a) is 25  $\mu\text{m}$ .

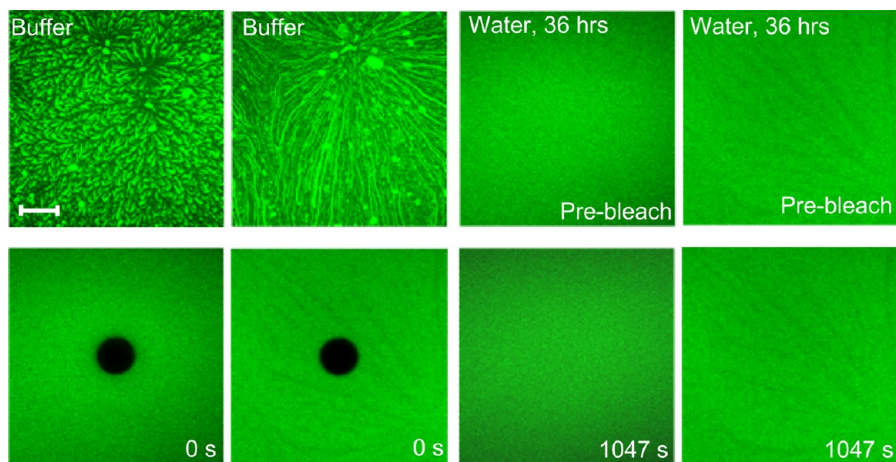


**Figure 5.** Excess lipid can be removed by washing to recover homogeneous SLBs. Fluorescence images of DOPC (left) and DOPC:DPPC:cholesterol 35:35:30 (mole) (right) systems before (“Buffer”) and after (“Water”) leaving them in water for 36 h. The flower- or tubelike structures disappear, giving way to homogeneous fluorescence and recovery after photobleaching characteristic of supported lipid bilayers. Time (in seconds) refers to the photobleaching experiments. Fluorescence intensity recovers after bleaching. The mobile fractions and diffusion coefficient values are presented in Table 1, labeled “after wash”. The incubation in water and FRAP experiments were performed at room temperature. Scale bar in (a) is 25  $\mu\text{m}$ .

shows no evidence of recovery (Figure 4b,c; Figure S4). Subsequently, low-intensity regions begin to appear in several places (white arrowheads in Figure 4b,c; see also Figure S4). We interpret these regions as bilayer patches. Weirich et al. reached a similar conclusion.<sup>10</sup> These regions expand, covering progressively more area. As they expanded, flowerlike structures began to form at their periphery. Once they reached the bleached region, the fluorescence intensity there started to recover up to the level of the bilayer regions, but no flowerlike structures were initially present in the bleached region even though they were present right next to it (Figure 4e–h and Figure S4). This indicates that the lipid material in the flowerlike structures comes from the liposomes adsorbed on the surface. If most of the lipid in these structures came from

solution, the bleached regions would be covered by the tubular structures to a similar extent as the regions around them. Therefore, what we are observing is a pathway for excess lipid leaving the surface during the bilayer formation process.

Notably, after some time, some flowerlike structures do appear in the bleached region as well (Figure 4g,h). Combined with the incomplete recovery of these structures noted above (Figures 2 and 3), this indicates that there is a pathway that allows new, fluorescent material from solution to reach the area where fluorescence was previously bleached.

Excess lipid material in these tubular or flowerlike structures could be removed by incubating the samples in water for 36 h. After such an incubation, SLBs that exhibited homogeneous fluorescence and complete recovery after photobleaching were

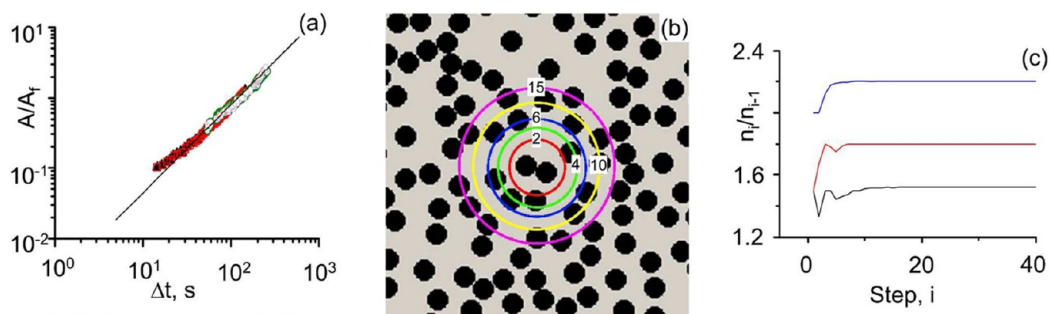


**Figure 6.** Following the growth of the bilayer patches. (a) A log–log plot of the scaled bilayer patch area vs time for the two patches visible in Figure 4 (black solid triangles and red open squares) and three of the patches visible in Figure S4 in the Supporting Information (brown, green, and blue open circles). Black solid line:  $A(t)/A_f \sim 0.0025t^{1.25}$ , where  $A_f$  is the area of a given patch at the time when the patches began to merge. This occurred at  $t = 88.23$  s for the patches shown in Figure S4 and  $t = 124.51$  s for the patches shown in Figure 4. The raw data is shown in Figure S8 in the Supporting Information and the scaling is further discussed in the main text. (b) This illustration shows liposomes (black circles) randomly arranged on the surface at a coverage of 0.38 and circular bilayer domains (colored open circles) that arise from liposome rupture. The red domain corresponds to the area covered by the lipids from the two liposomes present at its center. When formed, this domain will come into contact adsorbed liposomes, which will rupture, contributing to its area and forming the green domain. Numbers indicate the numbers of liposomes contributing to each domain (red, two liposomes; green, four liposomes; etc.). (c) This plot shows how the number of liposomes per bilayer domain evolves as the bilayer domain grows at different liposome surface coverages (0.38, black; 0.45, red; 0.55, blue). In each case, it was assumed that, upon rupturing, a liposome contributes an area  $4\pi R^2$  to the growing domain (no asymmetry). In each case, the first domain corresponded to two liposomes (nucleation). The number of liposomes,  $n$ , contributing to the domain at each subsequent growth step,  $i$ , was calculated from the liposome surface coverage as shown in (b).

left on the surface (Figure 5, Table 1). Sometimes defects did remain in the SLBs after such a wash (Figure 5, right column), but this observation was not reproducible. We think that the defects heal and can therefore not always be observed. In Figure S5 in the Supporting Information, it can be seen that the flowerlike structures remain unchanged during first  $\sim 17$  h of observation (Figure S5a–c), and that their number decreases sharply after another  $\sim 5$  h (Figure S5d,e), but that their appearance remains essentially unchanged (Figure S5e).

## DISCUSSION

In this study, we observe lipid material organized in extended flowerlike patterns coexisting with continuous SLBs (Figures 2–4). We prove that this material originates from the surface-adsorbed liposomes by following the recovery after bleaching as a function of time (Figure 4, and Figure S4 and Movie S3 in the Supporting Information), and therefore conclude that the appearance of these structures represents a channel for removing excess lipid from the surface during the SLB formation process.

On the one hand, the appearance of such structures is quite rare. Most common outcomes of the liposome–surface interactions are SLBs or layers of adsorbed liposomes.<sup>2,8–10,26–29</sup> There is a report of lipid tube formation at the edges of bilayer patches during SLB formation on mica,<sup>30</sup> but their presence was interpreted in terms of the propensity of the particular lipid mixtures to form tubes.<sup>31</sup> In our own studies, we found the flowerlike structures only in two out of the six different conditions (lipid and buffer compositions) that we characterized on  $\text{TiO}_2$ ; the results for other conditions will be presented elsewhere, but, in Figure S6 in the Supporting Information, we show that these structures do not form in the absence of calcium, that SLBs prepared from the DOPC:DPPC mixture without cholesterol exhibit no such structures (Figure S6a), and that such structures do not form from on glass from the lipid mixtures that lead to their formation on  $\text{TiO}_2$  (see Figure S7 in the Supporting Information). In other words, the parameters that are important for the formation of these

structures from DOPC are  $\text{TiO}_2$  and calcium, while DOPC:DPPC mixture also requires cholesterol.

On the other hand, as already mentioned in the Introduction, excess lipid material and its departure from the surface have been observed under rather common bilayer formation conditions.<sup>8,10,11</sup> Because of their very low solubility in aqueous buffers,<sup>32</sup> lipids would leave the surface in some sort of assemblies rather than molecule by molecule. Energetic considerations impose severe constraints on the geometry of lipid assemblies, resulting in the appearance of curvature.<sup>33,34</sup> In solution, this most commonly leads to spherical structures (vesicles). However, at a solid–liquid interface, the transition from a flat SLB stabilized by the adhesion to the surface to a soluble structure is more likely to proceed via elongated assemblies that maintain interaction with the surface, or with the bilayer edges on the surface. This is illustrated schematically in Figure 1. We therefore hypothesize that the structures we observe represent common intermediates in a pathway of lipid departure during SLB formation, but that the rate at which this occurs in most systems is too high for them to be observed. Indeed, the tubes observed by Ando et al. discussed above could only be visualized by the high-speed AFM methodology they developed.<sup>30</sup> The reason we were able to observe these structures in this study is most likely due to an energy barrier of some sort that drastically slows down their departure.

The observation that these structures can be removed by washing with a low ionic strength, Ca-free medium (water, Figure 5) supports the idea of the energy barrier. In contrast, surface-adsorbed liposomes cannot be removed by such washing steps. The origin of this energy barrier is unclear but is related to the way Ca modifies  $\text{TiO}_2$ –lipid interactions. The fact that it is the lipid–surface interactions that play a crucial role can be ascertained from the observation that, under identical conditions (same liposome solution in the same buffer), the flowerlike structures are seen on  $\text{TiO}_2$  but not on glass (Figure S7 in the Supporting Information). The crucial role of calcium is evident from the observation that the flowerlike structures do not appear in its absence (Figure S6a in

the Supporting Information). Lipid composition most likely determines the morphology of the assemblies because of the bending moduli and bilayer viscosity.

It is noteworthy that the overall appearance of the images is reminiscent of the Saffman–Taylor (fingering) instability that arises when a fluid flows through a porous media or when a less viscous fluid flows into a more viscous one (reviewed in ref 35). The flower- or tubelike structures appear to decorate the “fingers”. In other words, they appear at the edges of the growing bilayer patches, as illustrated schematically in Figure 1. Saffman–Taylor instability has been reported for the cases of spreading<sup>36</sup> and rupture<sup>37</sup> of giant liposomes, but until now not in the case of SLB formation. Possibly, the significant roughness of our TiO<sub>2</sub>-coated substrates contributes to this observation: the rms roughness of our surfaces was  $\sim 0.6$  nm (Figure S2 in the Supporting Information). For comparison, the roughness of native oxide on silicon wafers ranges between 0.05 and 0.1 nm.<sup>38–40</sup> Our own measurements yield a value of  $\sim 0.06$  nm for the roughness of the native oxide layer on the silicon wafers.

Further support for our hypothesis that these structures are common intermediates in a pathway of lipid departure during SLB formation can be gained from analyzing the growth of the bilayer patches. They are roughly circular and surprisingly well-defined (on the optical scale, Figure 4, and Figure S4 in the Supporting Information). Their appearance is rather different from the numerous and irregularly shaped (also on the optical scale) bilayer patches that are observed on SiO<sub>2</sub>.<sup>10</sup> This indicates that the conditions for nucleation of the bilayer regions are less common in the case of DOPC on TiO<sub>2</sub> than on SiO<sub>2</sub>; most likely, the liposome surface coverage required is higher on TiO<sub>2</sub> than on SiO<sub>2</sub>. It is also expected that, at a higher coverage, the rate of bilayer patch growth would be more isotropic, giving rise to a more circular shape. Higher coverage would also mean greater excess of lipid relative to the SLB.

The results of this analysis are shown in Figure 6 and Figure S8 in the Supporting Information. Patch area versus time plots for the bilayer patches shown in Figure 4 and Figure S4 are shown in Figure S8a in the Supporting Information. The time scales associated with these experiments are arbitrary, because bilayer formation started at different times relative to when the observations began. The bilayer patches are also of different size: they are much larger in Figure 4 than in Figure S4. To enable the comparison of these two sets, the area of each patch was scaled by its area at the point when the patches started to merge, and the time axes were aligned by offsetting them relative to each other to bring the scaled patch areas into register. The resulting plot is shown in Figure S8b in the Supporting Information, and the log–log version in Figure 6a. After the scaling, it becomes apparent that the rate of bilayer patch growth is independent of the domain size; i.e., the larger patches in Figure 4 grow at about the same rate as the smaller ones in Figure S4; their size is determined by their number, in other words, by the nucleation rate. On the other hand, the rate at which patches grow increases with time for all of them. This is exemplified by the power-law-like behavior where the scaled area grows as  $\sim t^{1.3}$  (Figure 6a, black solid line).

Spreading of lipid bilayers on surfaces has previously been analyzed by Rädler et al.<sup>36</sup> These authors studied the lipid bilayer spreading from a central source of lipids and found a behavior that was essentially parallel to the Brownian diffusion, with the radius of the growing patch  $r(t)$  proportional to the square root of time,  $t^{1/2}$ , implying a linear dependence of the

patch area on time, and a front velocity  $\sim t^{-1/2}$ . This was also observed more recently on nanostructured surfaces.<sup>41</sup> Here, we are dealing with a nucleation-and-growth-type phenomenon where new liposomes join the spreading bilayer domains at the periphery. Their rate of growth should, therefore, be controlled by the supply of the material, i.e., by the liposome surface coverage. At a given surface coverage, the rate should be constant. This process is examined in Figure 6b.

Figure 6b shows a surface with black filled circles representing liposomes placed at random locations at a coverage of  $\sim 0.38$ ; the coverage is defined as  $\Theta = N\pi R^2/A_{\text{surface}}$  where  $N$  is the number of liposomes on the surface,  $R$  is their radius, and  $A_{\text{surface}}$  is the surface area. Let us suppose that the two liposomes located in the center of Figure 6b rupture, giving rise to a bilayer patch indicated with a red circle (assuming that the area of the patch that arises from liposome rupture simply equals the surface area of the ruptured liposomes, in other words,  $A_{\text{patch}} = 4n\pi R^2$ , where  $n$  is the number of liposomes that contributed to the patch). As this red patch comes into contact with more adsorbed liposomes (one to its right and one below), they will also rupture: it is observed experimentally that adsorbed liposomes rupture upon contact with growing bilayer patches.<sup>2,26,28</sup> The lipid material from these liposomes will join the patch, giving rise to the green patch composed of the lipids from the four ruptured liposomes. This process will continue as long as the coverage of the liposomes on the surface is sufficiently high so that the growing patch can reach new liposomes. Simple analysis indicates that, for this propagation scenario to work, the surface coverage has to be at least 0.38. At lower coverage, the liposomes are too far apart, and patch growth ceases. For comparison, at a coverage of  $\sim 0.25$ , a layer of adsorbed liposomes contains the same amount of lipid material as a confluent lipid bilayer. This value was obtained by comparing the number of lipid molecules per unit area in an SLB with the number of lipid molecules per unit area in a layer of liposomes. This difference explains lipid excess at the surface during the SLB formation process.

In the above calculation, we ignored the fact that, for small liposomes, the area of the patch that arises from liposome rupture is smaller than expected based on the liposome area due to the significant difference in the number of lipids between the inner and the outer leaflets of the liposome. If we plug in a realistic number of lipids per liposome for a liposome with a 25 nm outer diameter, 3.7 nm bilayer thickness, and area per lipid of 0.72 nm<sup>2</sup>, the coverage required for propagation would be  $\sim 0.51$  and the equivalent bilayer coverage  $\sim 0.33$ . Lipid excess, defined as the ratio of lipid mass at the coverage required for propagation to that at the equivalent coverage, is in this case  $\sim 1.14$ . However, now these values depend on the liposome size. Because the asymmetry in the number of lipids between the two leaflets decreases with the liposome size, larger liposomes bring with them more lipids. For the outer diameter of 200 nm, the propagation coverage would be 0.38 and the equivalent bilayer coverage would be 0.26, yielding a lipid excess of 1.5. This increase of lipid excess with liposome size is confirmed experimentally as discussed in the Introduction.<sup>8</sup>

This “propagation coverage” should not be confused with the surface coverage required for nucleation of the bilayer patches, which we do not discuss in this work. It is simply an expression of geometrical constraints that operate at the surface: for the bilayer patch to continue growing, it has to be able to reach new liposomes.

We can compare the number of liposomes contributing to the growing patch at a given step with the number of liposomes contributing to that patch at the preceding step,  $\beta = N_i/N_{i-1}$ , where  $i$  is the step number ( $i = 0$  for the red patch,  $i = 1$  for the green one, and so on, Figure 6b). It turns out that, for a given coverage,  $\beta$  becomes constant after a few steps. Its value increases with coverage  $\Theta$  (Figure 6c). In other words, as the bilayer patch grows, it will come into contact with progressively greater numbers of liposomes, but that number increases by a constant factor with the size of the patch. The patch should then grow at a constant rate, rather than speed up, as we observe experimentally (Figure 6a).

In the preceding analysis, it was assumed that the surface coverage was constant during patch growth. If, on the other hand, liposomes continued to adsorb to the surface as the patches grew, the amount of material available to the growing patch would increase with time. This could explain the behavior of the patch area as a function of time we observe (Figure 6a). Supporting this conclusion is the appearance of the fluorescent flowerlike structures in the bleached area after some time (Figure 4g,h). We conclude that the final stages of the SLB formation—growth and coalescence of bilayer patches—entail an interplay between the departure of excess lipids on one hand and further liposome adsorption on the other. We should point out that Weirich et al. reported an increase in the liposome adsorption rate concurrent with the bilayer patch growth, which they attributed to the affinity of adsorbing liposomes for the bilayer edges.<sup>10</sup> Their observations are consistent with ours, although our interpretations differ somewhat.

Summarizing, we presented a simple model that accounts for our observations of the bilayer patch growth. This model furthermore allows us to conclude that, when SLB formation proceeds by collective rupture of liposomes, it requires a concentration of liposomes on the surface that contains more lipids than is contained in an SLB, explaining the lipid excess on the surface. Whether or not this is also true in the case of SLB formation that proceeds by the direct rupture of individual liposomes<sup>2,26,28</sup> is not clear and requires further investigation.

Last but not least, we tested the effect of the age of liposome suspension on the formation of bilayers and the patterns we observe. In Figure S7 in the Supporting Information, we used liposomes stored for 3 months after sonication. These liposomes yielded SLBs on both glass and TiO<sub>2</sub>, with the ones on TiO<sub>2</sub> exhibiting the flowerlike structures, and with the ones on glass showing a smooth appearance except for intense inclusions (presumably large liposomes that did not rupture).

We would like to finish with a historical note. To this day, SLB preparation remains an empirical procedure, where the results are obtained by trial and error. To the best of our knowledge, the first report of a zwitterionic bilayer prepared on TiO<sub>2</sub> was that by Starr and Thompson,<sup>42</sup> who used single-crystal rutile substrates, sonicated POPC liposomes, and low ionic strength media. Although there were some doubts about those results at the time,<sup>43,44</sup> these are very similar conditions to those we used here on a sputtered TiO<sub>2</sub> surface to form DOPC bilayers. At high ionic strength, liposomes made of low-melting POPC or DOPC phospholipids do not form bilayers on TiO<sub>2</sub>,<sup>44–46</sup> but surprisingly enough, their mixtures with high-melting phospholipids do: Tero et al. used sonicated liposomes containing mixtures of low-melting and high-melting phospholipids to prepare mixed SLBs on rutile (100),<sup>47</sup> and so did we in this study (Figure S6 in the Supporting Information). All of these results were obtained at neutral pH. The other

known route for preparing zwitterionic bilayers on TiO<sub>2</sub> is that due to Cho et al. that works at low pH (close to the IEP of TiO<sub>2</sub>).<sup>48,49</sup>

## CONCLUSIONS

In this study, we investigated late stages of SLB formation that involve the departure of excess lipid material from the surface. We observed excess of lipid material that remained associated with the bilayers in SLBs formed on TiO<sub>2</sub> in a Ca-containing buffer without monovalent ions from pure DOPC or DOPC:DPPC:cholesterol mixtures. This material could be removed by washing, leaving behind regular, homogeneous SLBs, indicating that there was an energy barrier preventing desorption. By analyzing bilayer patch growth rate, we came to the conclusion that the late stages of SLB formation involve both desorption of excess lipid and continued adsorption of liposomes from solution. This is a consequence of the limitations of the long-range transport of lipid material at the surface that arise from poor or nonexistent mobility of adsorbed liposomes. Departure of excess lipid during SLB formation appears to be a general phenomenon and is worth a systematic analysis to improve our understanding of lipid–surface interactions in general and SLB formation process specifically.

## ASSOCIATED CONTENT

### Supporting Information

A movie of the SLB formation process showing bilayer patch growth, and additional fluorescence microscopy and atomic force microscopy images of bilayers of different compositions and bare substrates, are available. This material is available free of charge via the Internet at <http://pubs.acs.org>.

## AUTHOR INFORMATION

### Corresponding Author

\*E-mail: [ilya.reviakine@kit.edu](mailto:ilya.reviakine@kit.edu).

### Present Addresses

<sup>¶</sup>National Center for Nanoscience and Technology, No. 11 ZhongGuanCun BeiYiTiao, 100190 Beijing, People's Republic of China.

<sup>||</sup>Institute of Functional Interfaces (IFG), Karlsruhe Institute of Technology (KIT), 76344 Eggenstein-Leopoldshafen, Germany.

### Notes

The authors declare no competing financial interest.

## ACKNOWLEDGMENTS

The authors are grateful to Dr. Luis Angel Yate (CIC biomaGUNE) for the help with the coating of the surfaces with TiO<sub>2</sub>, and for the XPS and ellipsometry analysis of the TiO<sub>2</sub> coatings; Ms. Marta Gallego, M.Sc. (CIC biomaGUNE), for expert technical assistance and helpful comments about this manuscript; and Prof. Alain Brison (University of Bordeaux, France) for enlightening discussions. Funding from the Department of Industry of the Basque Government (program ETORTEK) and from the Spanish Ministry of Science and Innovation (MICINN, ref CTQ2009-11245) to I.R. is also gratefully acknowledged.

## REFERENCES

(1) Sackmann, E. Supported membranes: Scientific and practical applications. *Science (New York, N.Y.)* **1996**, *271* (5245), 43–48.

- (2) Richter, R. P.; Berat, R.; Brisson, A. R. Formation of solid-supported lipid bilayers: An integrated view. *Langmuir* **2006**, *22* (8), 3497–3505.
- (3) Groves, J. T.; Dustin, M. L. Supported planar bilayers in studies on immune cell adhesion and communication. *J. Immunol. Methods* **2003**, *278* (1–2), 19–32.
- (4) Tanaka, M.; Sackmann, E. Supported membranes as biofunctional interfaces and smart biosensor platforms. *Phys. Status Solidi A: Appl. Mater.* **2006**, *203* (14), 3452–3462.
- (5) Hinrichsen, E. L.; Feder, J.; Jossang, T. Random packing of disks in 2 dimensions. *Phys. Rev. A* **1990**, *41* (8), 4199–4209.
- (6) Nagle, J. F.; Tristram-Nagle, S. Structure of lipid bilayers. *Biochim. Biophys. Acta: Rev. Biomembr.* **2000**, *1469* (3), 159–195.
- (7) Huang, C.; Mason, J. T. Geometric packing constraints in egg phosphatidylcholine vesicles. *Proc. Natl. Acad. Sci. U.S.A.* **1978**, *75* (1), 308–310.
- (8) Reimhult, E.; Zach, M.; Hook, F.; Kasemo, B. A multitechnique study of liposome adsorption on Au and lipid bilayer formation on SiO<sub>2</sub>. *Langmuir* **2006**, *22* (7), 3313–3319.
- (9) Richter, R. P.; Brisson, A. R. Following the formation of supported lipid bilayers on mica: A study combining AFM, QCM-D, and ellipsometry. *Biophys. J.* **2005**, *88* (5), 3422–3433.
- (10) Weirich, K. L.; Israelachvili, J. N.; Fyngenson, D. K. Bilayer edges catalyze supported lipid bilayer formation. *Biophys. J.* **2010**, *98* (1), 85–92.
- (11) Stroumpoulis, D.; Parra, A.; Tirrell, M. A kinetic study of vesicle fusion on silicon dioxide surfaces by ellipsometry. *AIChE J.* **2006**, *52* (8), 2931–2937.
- (12) Huang, C. H. Studies on phosphatidylcholine vesicles. Formation and physical characteristics. *Biochemistry* **1969**, *8* (1), 344–8.
- (13) Blume, A. Biological calorimetry - membranes. *Thermochim. Acta* **1991**, *193*, 299–347.
- (14) Kurrat, R.; Textor, M.; Ramsden, J. J.; Boni, P.; Spencer, N. D. Instrumental improvements in optical waveguide light mode spectroscopy for the study of biomolecule adsorption. *Rev. Sci. Instrum.* **1997**, *68* (5), 2172–2176.
- (15) Tejero, R.; Rossbach, P.; Keller, B.; Anitua, E.; Reviakine, I. Implant surfaces activated with plasma rich in growth factors: time of flight secondary ion mass spectrometry and principal component analysis study. *Langmuir* **2013**, *29*, 902–912.
- (16) Sittig, C. E. “Charakterisierung der Oxidschichten auf Titan und Titanlegierungen sowie deren Reaktionen in Kontakt mit biologisch relevanten Modellösungen”. Ph.D., ETH Zurich, 1998.
- (17) Rossetti, F. F.; Reviakine, I.; Textor, M. Characterization of titanium oxide films prepared by the template-stripping method. *Langmuir* **2003**, *19* (24), 10116–10123.
- (18) Axelrod, D.; Koppel, D. E.; Schlessinger, J.; Elson, E.; Webb, W. W. Mobility Measurement by Analysis of Fluorescence Photobleaching Recovery Kinetics. *Biophys. J.* **1976**, *16* (9), 1055–1069.
- (19) Soumpasis, D. M. Theoretical analysis of fluorescence photobleaching recovery experiments. *Biophys. J.* **1983**, *41* (1), 95–7.
- (20) Reviakine, I.; Bergsma-Schutter, W.; Brisson, A. Growth of protein 2-d crystals on supported planar lipid bilayers imaged in situ by AFM. *J. Struct. Biol.* **1998**, *121* (3), 356–362.
- (21) Müller, D. J.; Amrein, M.; Engel, A. Adsorption of biological molecules to a solid support for scanning probe microscopy. *J. Struct. Biol.* **1997**, *119* (2), 172–188.
- (22) Przybylo, M.; Sykora, J.; Humpolickova, J.; Benda, A.; Zan, A.; Hof, M. Lipid diffusion in giant unilamellar vesicles is more than 2 times faster than in supported phospholipid bilayers under identical conditions. *Langmuir* **2006**, *22* (22), 9096–9.
- (23) Rossetti, F. F.; Textor, M.; Reviakine, I. Asymmetric distribution of phosphatidyl serine in supported phospholipid bilayers on titanium dioxide. *Langmuir* **2006**, *22* (8), 3467–3473.
- (24) Kahya, N.; Schwille, P. How phospholipid-cholesterol interactions modulate lipid lateral diffusion, as revealed by fluorescence correlation spectroscopy. *J. Fluoresc.* **2006**, *16* (5), 671–8.
- (25) Oradd, G.; Westerman, P. W.; Lindblom, G. Lateral diffusion coefficients of separate lipid species in a ternary raft-forming bilayer: a Pfg-NMR multinuclear study. *Biophys. J.* **2005**, *89* (1), 315–20.
- (26) Reviakine, I.; Brisson, A. Formation of supported phospholipid bilayers from unilamellar vesicles investigated by atomic force microscopy. *Langmuir* **2000**, *16* (4), 1806–1815.
- (27) Muresan, A. S.; Lee, K. Y. C. Shape evolution of lipid bilayer patches adsorbed on mica: An atomic force microscopy study. *J. Phys. Chem. B* **2001**, *105* (4), 852–855.
- (28) Richter, R.; Mukhopadhyay, A.; Brisson, A. Pathways of lipid vesicle deposition on solid surfaces: A combined QCM-D and AFM study. *Biophys. J.* **2003**, *85* (5), 3035–3047.
- (29) Jass, J.; Tjarnhage, T.; Puu, G. From liposomes to supported, planar bilayer structures on hydrophilic and hydrophobic surfaces: An atomic force microscopy study. *Biophys. J.* **2000**, *79* (6), 3153–3163.
- (30) Ando, T. High-speed atomic force microscopy coming of age. *Nanotechnology* **2012**, *23* (6).
- (31) Reviakine, I.; Brisson, A. Streptavidin 2D crystals on supported phospholipid bilayers: Toward constructing anchored phospholipid bilayers. *Langmuir* **2001**, *17* (26), 8293–8299.
- (32) Israelachvili, J. *Intermolecular and Surface Forces*; Academic Press: San Diego, CA, 1997.
- (33) Lasic, D. D. The mechanism of vesicle formation. *Biochem. J.* **1988**, *256* (1), 1–11.
- (34) Lasic, D. D. A molecular model for vesicle formation. *Biochim. Biophys. Acta* **1982**, *692* (3), 501–502.
- (35) Homsy, G. M. Viscous fingering in porous-media. *Annu. Rev. Fluid Mech.* **1987**, *19*, 271–311.
- (36) Radler, J.; Strey, H.; Sackmann, E. Phenomenology and kinetics of lipid bilayer spreading on hydrophilic surfaces. *Langmuir* **1995**, *11* (11), 4539–4548.
- (37) Gozen, I.; Dommersnes, P.; Czolkos, I.; Jesorka, A.; Lobovkina, T.; Orwar, O. Fractal avalanche ruptures in biological membranes. *Nat. Mater.* **2010**, *9* (11), 908–12.
- (38) Richter, R. P.; Brisson, A. Characterization of lipid bilayers and protein assemblies supported on rough surfaces by atomic force microscopy. *Langmuir* **2003**, *19* (5), 1632–1640.
- (39) Lua, Y. Y.; Yang, L.; Pew, C. A.; Zhang, F.; Fillmore, W. J.; Bronson, R. T.; Sathyapalan, A.; Savage, P. B.; Whittaker, J. D.; Davis, R. C.; Linford, M. R. Polyelectrolytes as new matrices for secondary ion mass spectrometry. *J. Am. Soc. Mass Spectrom.* **2005**, *16* (10), 1575–82.
- (40) Crossley, A.; Sofield, C. J.; Goff, J. P.; Lake, A. C. I.; Hutchings, M. T.; Menelle, A. A study comparing measurements of roughness of silicon and SiO<sub>2</sub> surfaces and interfaces using scanning probe microscopy and neutron reflectivity. *J. Non-Cryst. Solids* **1995**, *187* (0), 221–226.
- (41) Furukawa, K.; Sumitomo, K.; Nakashima, H.; Kashimura, Y.; Torimitsu, K. Supported lipid bilayer self-spreading on a nanostructured silicon surface. *Langmuir* **2007**, *23* (2), 367–371.
- (42) Starr, T. E.; Thompson, N. L. Formation and characterization of planar phospholipid bilayers supported on TiO<sub>2</sub> and SrTiO<sub>3</sub> single crystals. *Langmuir* **2000**, *16* (26), 10301–10308.
- (43) Ajo-Franklin, C. M.; Kam, L.; Boxer, S. G. High refractive index substrates for fluorescence microscopy of biological interfaces with high z contrast. *Proc. Natl. Acad. Sci. U.S.A.* **2001**, *98* (24), 13643–13648.
- (44) Rossetti, F. F.; Bally, M.; Michel, R.; Textor, M.; Reviakine, I. Interactions between Titanium Dioxide and Phosphatidyl Serine-containing Liposomes: Formation and Patterning of Supported Phospholipid Bilayers on the Surface of a Medically Relevant Material. *Langmuir* **2005**, *21*, 6443–6450.
- (45) Reviakine, I.; Rossetti, F. F.; Morozov, A. N.; Textor, M. Investigating the properties of supported vesicular layers on titanium dioxide by quartz crystal microbalance with dissipation measurements. *J. Chem. Phys.* **2005**, *122* (20), 204711–204718.
- (46) Reimhult, E.; Hook, F.; Kasemo, B. Vesicle adsorption on SiO<sub>2</sub> and TiO<sub>2</sub>: Dependence on vesicle size. *J. Chem. Phys.* **2002**, *117* (16), 7401–7404.

(47) Tero, R.; Ujihara, T.; Urisu, T. Lipid bilayer membrane with atomic step structure: supported bilayer on a step-and-terrace TiO<sub>2</sub>(100) surface. *Langmuir* **2008**, *24* (20), 11567–76.

(48) Cho, N. J.; Frank, C. W. Fabrication of a planar zwitterionic lipid bilayer on titanium oxide. *Langmuir* **2010**, *26* (20), 15706–15710.

(49) Cho, N. J.; Jackman, J. A.; Liu, M.; Frank, C. W. pH-driven assembly of various supported lipid platforms: a comparative study on silicon oxide and titanium oxide. *Langmuir* **2011**, *27* (7), 3739–3748.

Supporting Information: Nanoscale Departures: Excess Lipid  
Leaving the Surface During Supported Lipid Bilayer Formation.

Ling Zhu<sup>a,b</sup>, Danijela Gregurec,<sup>a,b</sup> and Ilya Reviakine<sup>a,c,d,\*</sup>

AUTHOR ADDRESS

<sup>a</sup> Biosurfaces, CIC biomaGUNE, Paseo Miramón 182, San Sebastián, 20009, Spain

<sup>b</sup> Department of Biochemistry and Molecular Biology, University of the Basque Country,  
28940 Leioa, Spain

<sup>c</sup> School of Engineering, University of the Basque Country, 48013 Bilbao, Spain.

<sup>d</sup> Current address: Institute of Functional Interfaces (IFG), Karlsruhe Institute of  
Technology (KIT), 76344 Eggenstein-Leopoldshafen, Germany

\* Corresponding author: Ilya.Reviakine@kit.edu

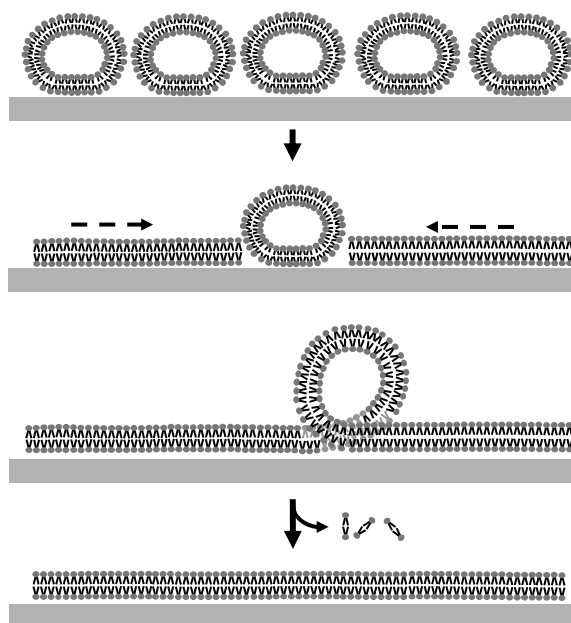
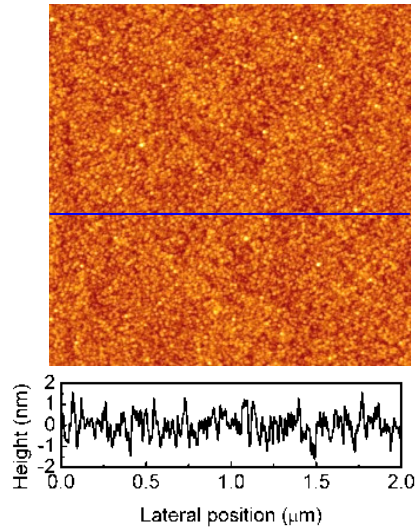


**Figure S1: Supported Lipid Bilayer Formation.**

Liposomes adsorbed on a surface (top) rupture to form supported lipid bilayers (SLBs, bottom). However, a layer of adsorbed liposomes may contain more lipids than can be accommodated in an SLB. Lipid excess is removed from the surface in some manner during the SLB formation process. Middle images illustrate schematically one possibility, also illustrated in Figure 1 in the main text of the manuscript, where a liposome is “caught” in a cleft between two bilayer patches. The form, in which lipids are removed, is not clear. In this study we have, however, been able to visualize structures with elongated morphologies that are associated with the bilayers in two systems: DOPC and DOPC : DPPC : cholesterol (35 : 35 : 30 mol%) on TiO<sub>2</sub> in a buffer containing 2 mM Ca<sup>2+</sup> but no other ions (except for the HEPES buffer itself). These structures can be removed by washing with water, suggesting that they are trapped on the surface kinetically.

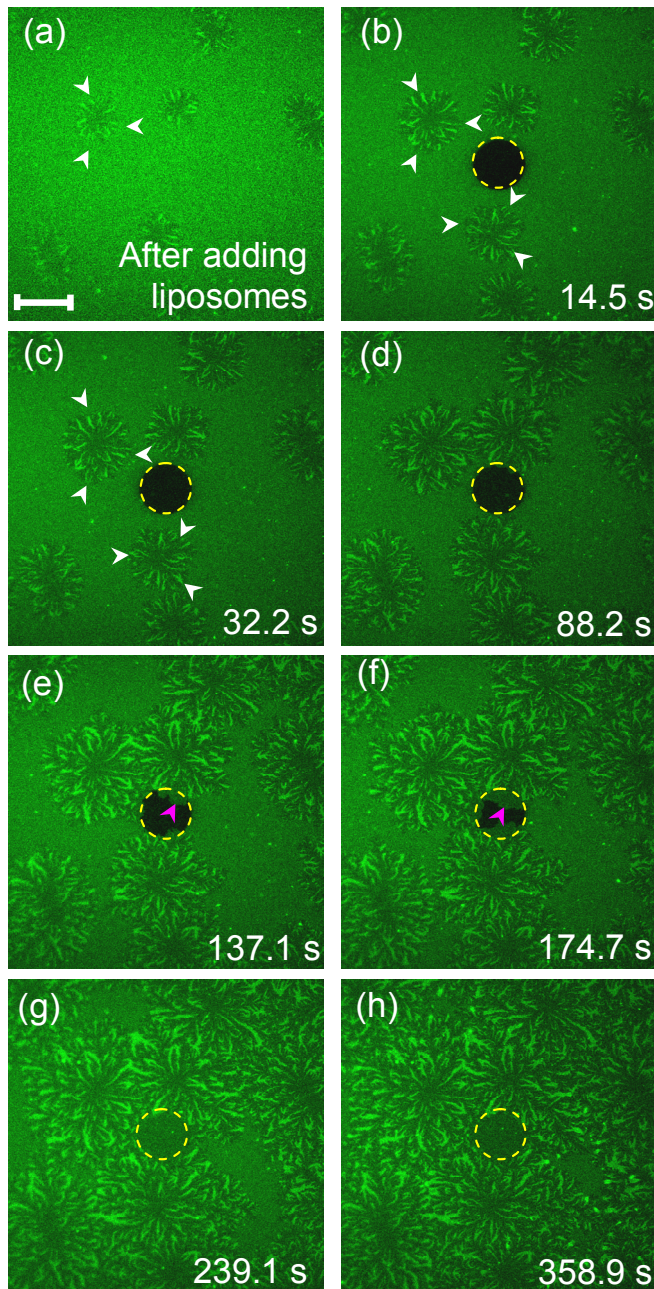
**Figure S2: TiO<sub>2</sub>-coated glass surface analyzed by AFM.**



A  $2 \times 2 \mu\text{m}^2 \times 10 \text{ nm}$  tapping mode AFM image of the TiO<sub>2</sub>-coated glass surface. The blue line indicates where the height profile shown below the image was taken. Surface rms (root mean square) roughness was measured with the Nanoscope software to be  $\sim 0.6 \text{ nm}$ .

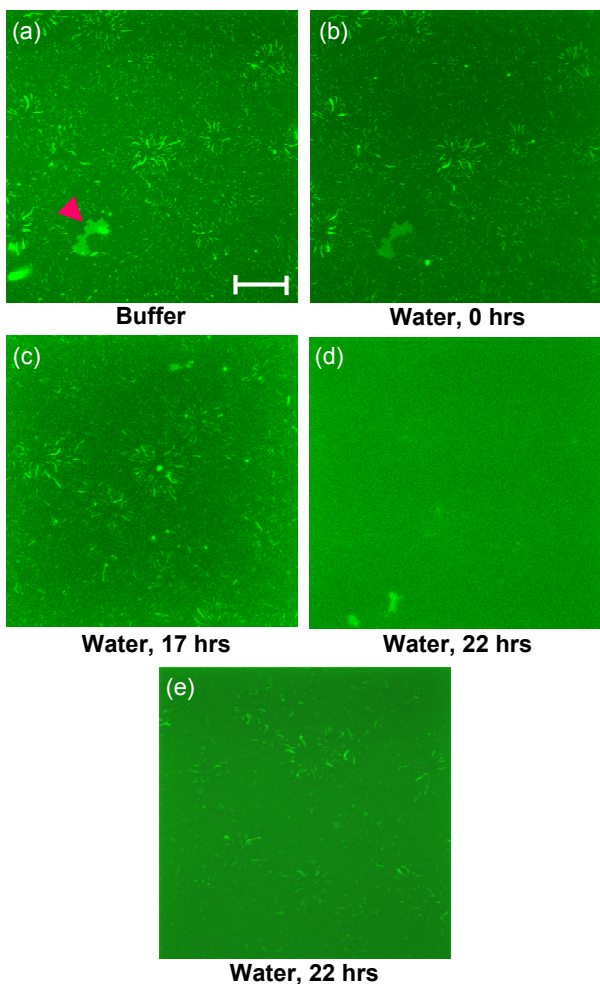
**Movie S3:** Sequence of fluorescence images acquired with pure DOPC liposomes in a buffer containing 10 mM HEPES and 2 mM CaCl<sub>2</sub> at 60 °C (same experiment as shown in Figure 3 in the main text). A circular area where fluorescence intensity was bleached appears in the middle of the images. Initially, the fluorescence intensity does not recover, indicating that initially, the surface is covered by adsorbed liposomes. Two darker, nearly circular regions appear to the top right and bottom left of the bleached area. They grow and develop flower-like structures at their periphery. A third such region grows at the bottom of the observed area and a fourth appears in the bottom left corner towards the end of the movie. The images are  $142 \times 142 \mu\text{m}^2$ , and a frame was recorded every 1.97 seconds, making the entire sequence 203 seconds long. For convenience, it is displayed at a  $\sim 20\times$  faster rate.

**Figure S4:** A sequence of fluorescence images capturing the growth of bilayer domains



in DOPC on  $\text{TiO}_2$  in 10 mM HEPES 2 mM  $\text{CaCl}_2$  pH 7.4 buffer at 60 °C. Images are  $142 \times 142 \mu\text{m}^2$ . Several bilayer domains are indicated with white arrowheads. Bleached spot is indicated with a yellow dashed circle. Note that initially, there is no recovery in the bleached spot, indicating that initially, a layer of liposomes is present on the surface. The recovery commences when the growing lipid bilayer patches reach the bleached area (purple arrowheads). Note that there are no flower-like structures in the bleached area. Scale bar in (a) is 25  $\mu\text{m}$ .

**Figure S5:** Removal of Excess Lipid Material in Water.



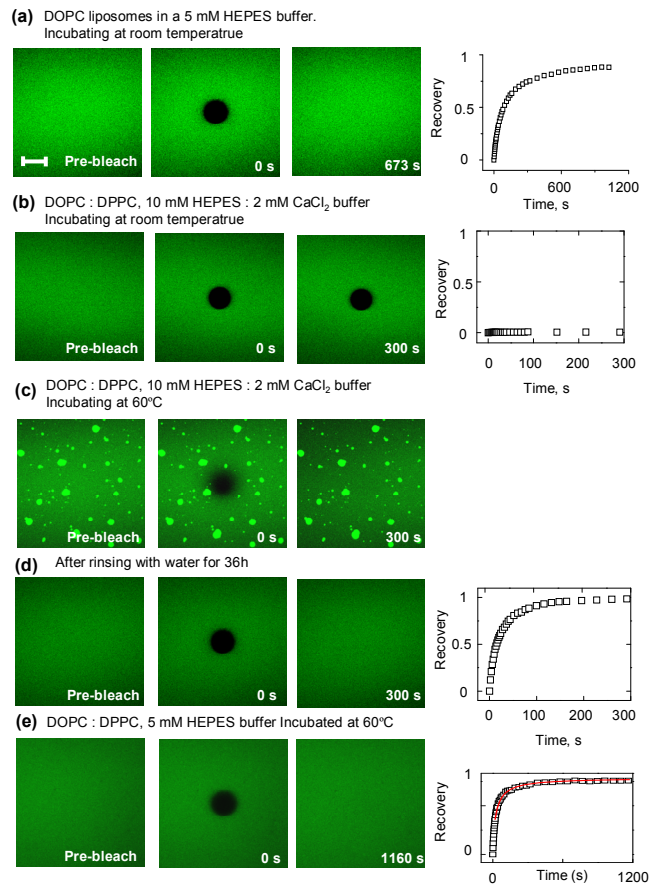
300  $\mu\text{l}$  of 2.5 mg/ml solution of sonicated DOPC liposomes containing 1% NBD-PC in buffer containing 10 mM HEPES and 2 mM  $\text{CaCl}_2$  was incubated with the freshly cleaned  $\text{TiO}_2$  surface overnight and rinsed with the same buffer (a). The samples were subsequently rinsed 10 $\times$  with Nanopure water, each time by repeatedly adding and withdrawing 150  $\mu\text{l}$  volume of liquid (b). Same sample after 17 hrs of incubation is shown in (c). The image in (c) was followed by an additional rinse with water (10 $\times$ ). (d) and (e) show two

different areas of the same sample after an additional 5 hrs of incubation in water. Purple arrowhead in (a) points to an area of adsorbed liposomes. Scale bar in (a) is 25  $\mu\text{m}$ .

There are essentially no changes to the structures present on the surface in the first 17 hrs of incubation with water, and then a rather abrupt decrease in their number in the next five hours. Note that the remaining structures do not significantly change in appearance (c.f. (c) and (e)). Note also, that a very high lipid concentration was used in this experiment (2.5 mg/ml as opposed to 0.36 mg/ml used in all other experiments reported in this study), without a significant effect on the appearance of the lipid assemblies. The

small solution volume (0.3 ml instead of 1 ml) used in this experiment was due to the use of a smaller fluid cell.

**Figure S6:** (a) A bilayer prepared on  $\text{TiO}_2$  from DOPC liposomes in 5 mM HEPES



buffer. The curve on the right represents the recovery of the fluorescence intensity after bleaching.

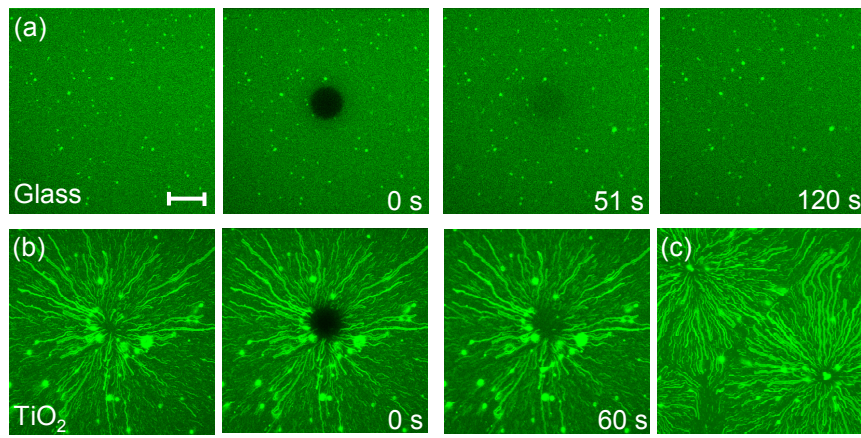
(b) A supported vesicular layer that forms from DOPC : DPPC system in the 10 mM HEPES : 2 mM  $\text{CaCl}_2$

buffer before heating to 60 °C. No recovery of fluorescence intensity is observed. (c) A bilayer is formed in the same sample as shown in (b) after heating to 60 °C, but it contains

bright structures on top. (d) The same sample as in (c) after incubating in

water for 36 hrs results in a smooth, homogeneous bilayer. (e) In the absence of Ca (5 mM HEPES buffer), DOPC : DPPC lipid mixture leads to a homogeneous bilayer. The images are  $142 \times 142 \mu\text{m}^2$ . Scale bare in (a) is 25  $\mu\text{m}$ .

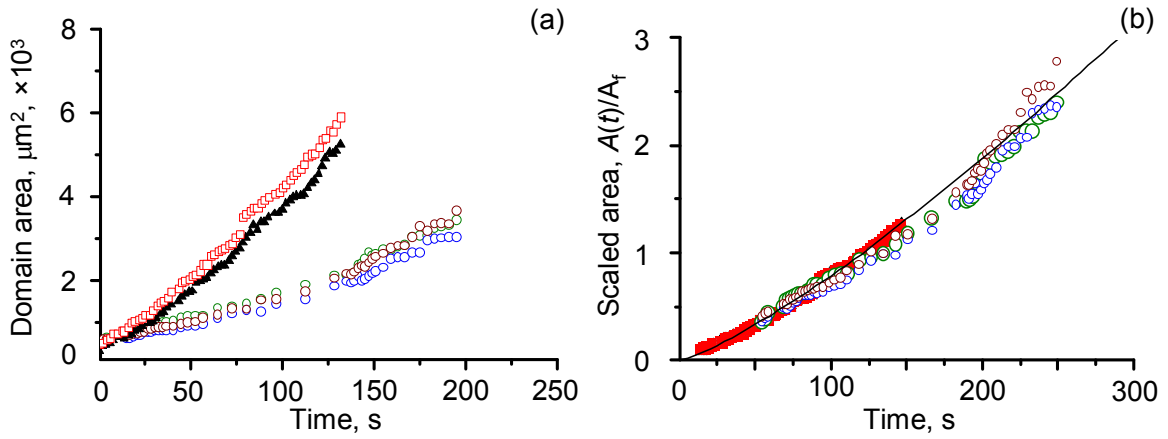
**Figure S7:** Effect of Liposome Age and Surface on the Morphology of the Lipid Assemblies.



In this experiment, an old liposome solution (~ three month) was used on glass (a) and TiO<sub>2</sub> (b, c). The image in (c) is from the same

sample as (b) but from a different area. The scale bar in (a) is 25  $\mu\text{m}$ . In both cases, liposome concentration was 0.46 mg/ml and in both cases the buffer contained 5 mM HEPES and 2 mM CaCl<sub>2</sub>. Firstly, from the recovery of fluorescence, it can be seen that bilayers formed on both surfaces. Secondly, the bilayer on TiO<sub>2</sub> coexists with the flower-like assemblies, while the bilayer on glass does not. It is relatively smooth, except for inclusions which probably result from the old liposome suspension being used.

**Figure S8: Analysis of the bilayer domain growth rates.**



(a) The area vs. time plot for the bilayer domains shown in Figure 3 (black solid triangles and red open squares) and three of the domains visible in Figure S4 (brown, green and blue open circles).

(b) The scaled area,  $A_s(t) = A(t)/A_f$ , was calculated by dividing the area at each time point by the area at the point when domains began to merge,  $A_f$ , which occurred at  $t = 88.23$  s for the domains shown in Figure S4 and  $t = 124.51$  s for the domains shown in Figure 3. Furthermore, the two experiments were started at different times relative to the time when membrane domains nucleated. The two data sets were brought into register by adding a constant  $t_0 = 53.8$  s to the time at which images shown in Figure S5 were recorded, such that the scaled areas  $A_s(t+t_0)$  for that experiment were similar to the scaled areas  $A_s(t')$  for the domains shown in Figure 3 when  $t' = t + t_0$ . Black solid line:  $A(t)/A_f \sim 0.0025t^{1.25}$ .

Figure 6 shows the log-log plot of the plot shown in (b).